

# VISREF: Visual Refocusing while Thinking Improves Test-Time Scaling in Multi-Modal Large Reasoning Models

Soumya Suvra Ghosal<sup>1\*</sup> Youngeun Kim<sup>2\*</sup> Zhuowei Li<sup>2</sup> Ritwick Chaudhry<sup>2</sup> Linghan Xu<sup>2</sup>  
 Hongjing Zhang<sup>2</sup> Jakub Zablocki<sup>2</sup> Yifan Xing<sup>2</sup> Qin Zhang<sup>3†</sup>

<sup>1</sup>University of Maryland, College Park <sup>2</sup>Amazon <sup>3</sup>Physion Labs

sgghosal@umd.edu {youngeuk, zhuoweli, ritwic, linghanx, zhongji, jzablock, yifax}@amazon.com qin@physionlabs.ai

## Abstract

Advances in large reasoning models have shown strong performance on complex reasoning tasks by scaling test-time compute through extended reasoning. However, recent studies observe that in vision-dependent tasks, extended textual reasoning at inference time can degrade performance as models progressively lose attention to visual tokens and increasingly rely on textual priors alone. To address this, prior works use reinforcement learning (RL)-based fine-tuning to route visual tokens or employ refocusing mechanisms during reasoning. While effective, these methods are computationally expensive, requiring large-scale data generation and policy optimization. To leverage the benefits of test-time compute without additional RL fine-tuning, we propose *VisREF*, a visually grounded test-time scaling framework. Our key idea is to actively guide the reasoning process by re-injecting a coreset of visual tokens that are semantically relevant to the reasoning context while remaining diverse and globally representative of the image, enabling more grounded multi-modal reasoning. Experiments on three visual reasoning benchmarks with state-of-the-art multi-modal large reasoning models demonstrate that, under fixed test-time compute budgets, *VisREF* consistently outperforms existing test-time scaling approaches by up to 6.4%.

## 1. Introduction

Multi-modal Large Reasoning Models (MLRMs) [4, 9, 53] have demonstrated remarkable capabilities by extending Chain-of-Thought reasoning [47] to vision-language reasoning tasks [32, 57]. By generating explicit thinking traces before producing final answers, these models achieve strong performance on benchmarks requiring mathematical reasoning [32], scientific problem-solving [57], and general

\*Equal contribution. This work was done during Soumya Suvra Ghosal’s internship at AWS AI Labs.

†Work done while at AWS AI Labs.

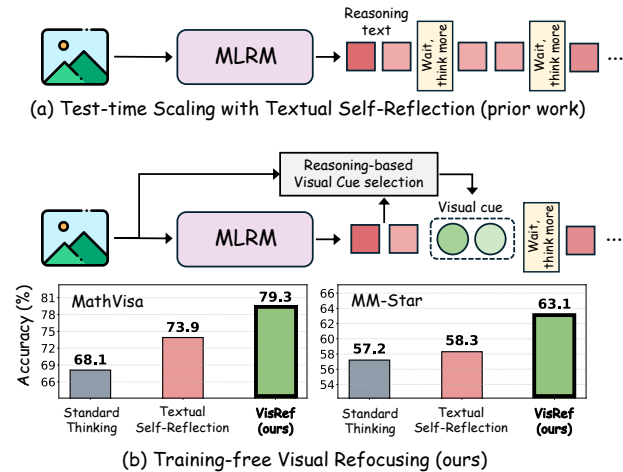


Figure 1. Illustration comparing our approach with prior test-time scaling methods. (a) Textual self-reflection-based test-time scaling [2, 34] extends reasoning by encouraging the model to think longer, but progressively loses grounding in the visual input as the reasoning chain grows. (b) Training-free Visual Refocusing (ours) dynamically selects and re-injects reasoning-relevant visual cues during inference, effectively restoring visual grounding without retraining and yielding substantial accuracy gains on the MathVista and MM-Star benchmarks with InternVL3.5-8B.

multi-modal understanding [8]. However, a critical limitation emerges: for several vision-critical tasks, as these models generate longer reasoning traces, their attention to visual information progressively diminishes [9, 51]. Visual tokens become increasingly diluted in the expanding context window, causing the model to rely more on textual priors rather than grounding its reasoning in actual image content [29, 65].

This dilution of attention to visual tokens in MLRMs stands in stark contrast to human problem-solving. When humans reason about a multi-modal task, whether solving a geometry problem, interpreting a chart, or analyzing a diagram, they naturally alternate between examining the image and working through their reasoning, returning to verify visual

details whenever uncertainty arises [5, 12]. This interplay between perception and reasoning, where visual information grounds abstract thinking and reasoning guides visual attention, is fundamental to robust visual reasoning. Current MLRMs, however, lack this feedback loop: once visual tokens are processed initially, they progressively fade from the model’s attention as textual reasoning dominates.

Recent studies have tried to address visual dilution through two main directions. The first employs reinforcement learning (RL) fine-tuning to teach models explicit “look-back” behaviors [9, 51]. While effective, these methods are computationally expensive, and require curating large-scale annotated datasets, limiting their scalability. The second direction, test-time scaling, allocates additional inference compute to refine reasoning [2, 34, 38]. These methods generate longer reasoning chains or employ self-verification during thinking. However, existing test-time scaling approaches remain predominantly text-centric: they extend textual reasoning but fail to actively maintain visual grounding throughout the process. As the reasoning chain grows longer, visual information continues to fade, limiting their effectiveness on vision-dependent reasoning tasks [9].

This gap between costly training-based solutions and ineffective text-centric test-time scaling motivates our central question: *Can we restore visual grounding entirely at test time, without any retraining?* To this end, we introduce VISREF, a training-free framework that adaptively reinjects carefully selected visual tokens at each reasoning step, allowing the model to refocus on relevant visual content as its reasoning evolves (Fig. 1). This approach mimics the human strategy of alternating between visual examination and abstract reasoning, but does so purely at test time, requiring no specialized training data and RL fine-tuning. The core challenge is determining which visual tokens to reinject at each step, as naively reinjecting all tokens is computationally prohibitive and can introduce redundant information. We formulate this as an optimization problem: selecting a core-set that is both relevant to the current reasoning state and diverse in its visual coverage. We employ Determinantal Point Processes (DPPs) [28], which provide a principled and tractable mechanism to balance these two objectives. Furthermore, we introduce an entropy-based stopping criterion to prevent unbounded computation, terminating reasoning once the model achieves sufficient confidence.

We validate VISREF on three challenging visual-reasoning benchmarks (Section 5): MathVista [32], MM-Star [8], and MathVision [43]. Experiments across state-of-the-art MLRMs, including InternVL-3.5 [44], Qwen-3-VL [4], and SAIL-VL2 [56] demonstrate consistent and significant improvements. For instance, on MathVision with SAIL-VL2, VISREF achieves 7.5% absolute accuracy improvement over standard thinking and 5.4% over textual self-reflection [34]. Furthermore, we demonstrate that VISREF scales favorably

with increased test-time compute: when generating multiple parallel reasoning chains under a fixed token budget [19, 46], VISREF consistently achieves superior performance for any given computational budget across all benchmarks. These results establish training-free visual refocusing as a practical and generalizable approach to maintaining visual grounding. We summarize our contributions as follows:

- We propose VISREF, a training-free framework for adaptive visual refocusing that dynamically reinjects visual information during test-time reasoning without modifying model parameters.
- We leverage a DPP-based formulation for selecting visual tokens, ensuring the selected subset is both relevant to the current reasoning state and provides diverse visual coverage in the feature space.
- We provide comprehensive empirical validation on challenging benchmarks (MathVista, MM-Star, MathVision) and state-of-the-art models (InternVL-3.5, Qwen3-VL, SAIL-VL2), demonstrating that VISREF significantly outperforms existing text-centric test-time scaling approaches.

## 2. Related Works

**Multi-modal Large Reasoning Models (MLRMs).** The success of Chain-of-Thought (CoT) reasoning in LLMs [47] spurred its adaptation to the multi-modal domain through Multimodal Chain-of-Thought (MCoT) [16, 37, 63]. Initial MCoT methods relied on prompt engineering to elicit step-by-step reasoning traces. However, these short, reactive chains often proved insufficient for complex, real-world tasks requiring long-horizon planning [57, 62, 64]. To address this gap, recent research has shifted toward using reinforcement learning [21] to instill more deliberate and methodologically structured reasoning processes. This paradigm shift, notably influenced by work like DeepSeek-R1 [21], has inspired a new generation of MLRMs designed for deeper reasoning [4, 6, 13, 20, 24, 36, 41, 42, 44, 50, 53, 54].

**Test-time Scaling in Reasoning Models.** Recent work by Muennighoff et al. [34] introduced the concept of budget forcing to replicate the test-time scaling behavior observed in o1 models [35]. Another recent approach, L1 [2], proposed length-controlled policy optimization, providing precise control over the length of the reasoning trace during generation. Yang et al. [52] introduced a thinking-optimal scaling strategy, training models to adapt dynamically to different levels of reasoning effort depending on the test-time compute budget. Recently, a lot of studies have also focused on fine-tuning models to think efficiently according to task complexity [3, 14, 23, 26, 31, 59, 61]. However, a growing body of evidence indicates that simply extending the thinking process at test time can lead to oscillatory performance [19, 22, 48]. In the multimodal setting, Chu et al. [9] observed a similar trend: as reasoning length increases, attention to visual

tokens degrades, harming visual grounding.

**Visual refocusing in MLRMs.** Recent works [9, 51, 58] has emphasized the need to refocus on visual tokens during multi-modal reasoning, as extended inference often leads to degradation of visual grounding. Chu et al. [9] address this by fine-tuning models with explicit “look-back” or “reflect” mechanisms that copy or route visual tokens during inference. Similarly, Yang et al. [51] proposed an implicit refocusing scheme using specialized supervision to encourage models to revisit image context mid-reasoning. Another emerging line of research explores enhancing multi-modal models through the integration of external visual tools. Several approaches incorporate zoom, cropping, or agent-based utilities [25, 39, 58, 60], or leverage advanced vision modules through supervised fine-tuning or reinforcement learning to enable tool-using behaviors [10, 18, 60]. While above-mentioned methods successfully enhance visual grounding, they typically require specialized dataset construction, model retraining, tool-calling, or architectural modifications. In contrast, our framework, VISREF, enables efficient and adaptive visual refocusing purely at test time with minimal overhead, making it plug-and-play for any pre-trained MLRM.

### 3. Preliminaries

**Mathematical formulation of thinking process.** Formally, an MLRM-generated thinking process can be expressed as:

$$x_{\text{input}} \rightarrow z \rightarrow y, \quad (1)$$

where  $x_{\text{input}} = [I, T]$  denotes the input, with  $I \in \mathcal{I}$  the visual input (e.g., image) and  $T = (t_1, t_2, \dots, t_P)$  the textual prompt consisting of  $P$  tokens ( $t_i \in \mathcal{M}$  for vocabulary  $\mathcal{M}$ ). The model first produces a reasoning (or thinking) trace  $z \sim \pi_{\theta}(\cdot | x_{\text{input}})$  and then a final answer  $y \sim \pi_{\theta}(\cdot | x_{\text{input}}, z)$ . The RL objective for training reasoning models is:

$$\max_{\theta} \mathbb{E}_{\substack{x_{\text{input}}, z \sim \pi_{\theta}(\cdot | x_{\text{input}}), \\ y \sim \pi_{\theta}(\cdot | x_{\text{input}}, z)}} [R(x_{\text{input}}, y)], \quad (2)$$

where  $\pi_{\theta}$  is the parameterized model and  $R(x_{\text{input}}, y)$  represents the true reward function (e.g., an indicator to check if  $y$  is correct or not), which is obtained once the policy generates the final response  $y$ .

**Textual self-reflection in reasoning models.** Textual self-reflection [34] extends the thinking process as:

$$x_{\text{input}} \rightarrow z_1 \rightarrow z_2 \rightarrow \dots \rightarrow z_k \rightarrow y,$$

where, given the prompt  $x_{\text{input}}$ , the model first generates an initial reasoning step  $z_1 \sim \pi_{\theta}(\cdot | x_{\text{input}})$ . Rather than producing the final answer immediately, the model is prompted to continue reasoning using special instruction tokens (e.g., “Wait”, “Think more”), denoted by  $c$ . Subsequent reasoning

steps are sampled iteratively as  $z_t \sim \pi_{\theta}(\cdot | x_{\text{input}}, z_{1:t-1}, c)$  for  $t = 2, \dots, k$ , until the model generates final response as  $y \sim \pi_{\theta}(\cdot | x_{\text{input}}, z_{1:k}, c)$ . For brevity, we omit explicit mention of  $c$  in the conditioning and denote the thinking traces in the condition as  $y \sim \pi_{\theta}(\cdot | x_{\text{input}}, z_{1:k})$ .

## 4. Proposed Framework

**Problem Setup.** Recent studies [9, 51] have observed that in vision-dependent reasoning tasks [32, 57], scaling test-time compute by extending textual reasoning often leads to a dilution of visual information, weakening the influence of visual tokens and inducing visual hallucinations [15, 30, 65]. To mitigate this issue, prior works [9, 51] employed RL fine-tuning [21] to enable models to autonomously decide when and how to refocus on visual input during reasoning. While empirically effective, RL-based approaches are computationally intensive and require costly data curation. This motivates a central question: *Can we achieve adaptive visual refocusing entirely at test time, without additional fine-tuning?*

We address this challenge by introducing VISREF, a training-free framework that dynamically reintegrates visual information during thinking. Our key insight is to augment the textual reasoning trace by adaptively reinjecting relevant visual tokens at each step, ensuring the model maintains grounded visual context throughout its reasoning process.

Formally, given an image-text input  $x_{\text{input}} = [I, T]$ , let  $\mathcal{V} = \{v_1, v_2, \dots, v_N\}$  denote the set of  $N$  visual token embeddings extracted from image  $I$ , where each  $v_i \in \mathbb{R}^d$  is a  $d$ -dimensional vector. At reasoning step  $k$ , the visual-integrated reasoning trajectory can be expressed as:

$$\tau_{1:k} = \{(z_1, V_1), (z_2, V_2), \dots, (z_k, V_k)\}, \quad (3)$$

where  $z_i$  denotes the textual reasoning step at step  $i$  and  $V_i \subseteq \mathcal{V}$  represents the subset of visual tokens reinjected at that step. The model continues the reasoning process until a stopping condition is met and generates the final answer as  $y \sim \pi_{\theta}(\cdot | x_{\text{input}}, \tau_{1:k})$ . The stopping criterion is important as indefinitely reinjecting tokens may degrade performance due to overthinking [19, 38], while premature stopping can yield incomplete reasoning and incorrect predictions.

### 4.1. Our Approach: VISREF

Enabling autonomous visual refocusing during reasoning presents two key challenges: (1) *visual token selection*: identifying which subset of visual tokens to re-inject at each step, and (2) *stopping criterion*: determining when to terminate reasoning and generate the final answer. We address challenge 1 in 4.1.1 and challenge 2 in 4.1.2. The overall method is illustrated in Fig. 2.

#### 4.1.1. Identifying Optimal Visual Token Subsets

A naive solution to mitigate visual token dilution would be reinjecting all  $N$  visual tokens at every reasoning step. How-

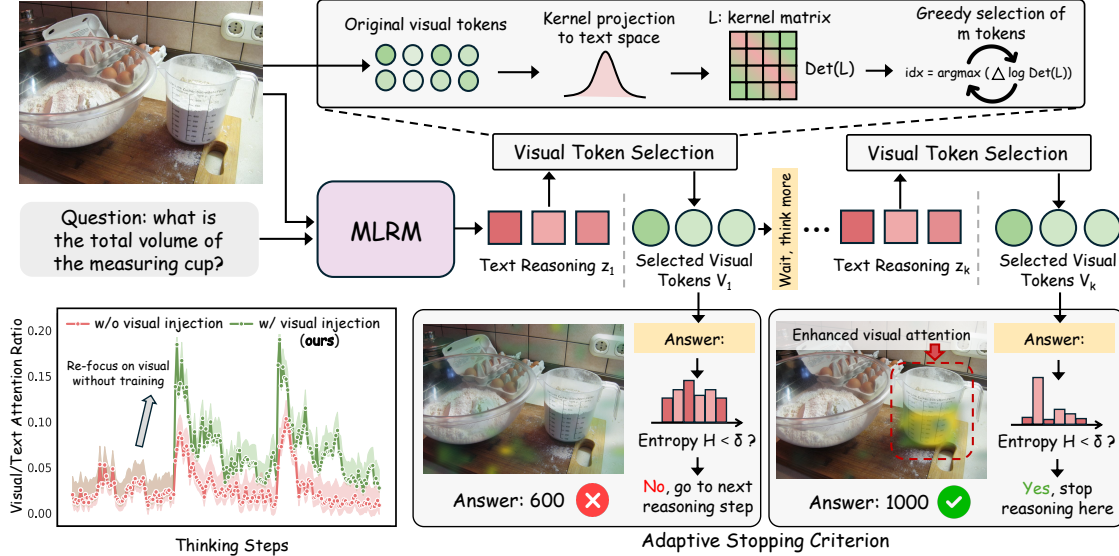


Figure 2. **Overview of VisREF.** Given an image-text input, VisREF enables multi-modal large reasoning models (MLRMs) to maintain visual grounding throughout the reasoning process without retraining. At each reasoning step, the model projects visual tokens into the textual reasoning subspace and selects a subset of reasoning-relevant tokens via a determinantal point process (DPP)-based criterion. The selected tokens are then reinjected to guide subsequent reasoning. This iterative process continues until the entropy of the model’s answer distribution falls below a confidence threshold  $\delta_{\text{entropy}}$ , forming an adaptive stopping criterion. The bottom-left plot shows the visual-to-text attention ratio across reasoning steps. As shown, our method maintains a higher level of visual attention (green curve) by reinjecting a carefully selected coreset of visual tokens, whereas text-based self-reflection (red curve) exhibits a more rapid decline in visual attention, consistent with prior observations [9, 51]. Example shown uses InternVL-3.5-8B on MathVista.

ever, this strategy is computationally prohibitive in practice, significantly increasing context length and inference latency. For example, using InternVL-3.5-8B [44] on MathVista [32], the number of visual tokens per image averages approximately  $3\times$  the text tokens generated in each reasoning step (e.g.,  $\sim 1,772$  visual tokens vs.  $\sim 615$  text tokens), and appending all visual tokens leads to a  $2.3\times$  increase in inference latency compared to text-only reasoning. Hence, to address this computational bottleneck, we seek to select a coreset of visual tokens  $V_k \subseteq \mathcal{V}$  at each reasoning step  $k$  that maximizes the expected reward of the final answer. Formally, the optimal coreset satisfies:

$$V_k^* = \arg \max_{V_k \subseteq \mathcal{V}} \mathbb{E}_{\substack{y \sim \pi_\theta(\cdot | x_{\text{input}}, \tau_{1:k}), \\ z_{k+1:k} \sim \pi_\theta(\cdot | x_{\text{input}}, \tau_{1:k-1}, z_k, V_k)}} [R(x_{\text{input}}, y)], \quad (4)$$

where  $\tau_{1:k-1} = \{(z_1, V_1), \dots, (z_{k-1}, V_{k-1})\}$  denotes the visually integrated reasoning trajectory up to step  $k-1$ . The objective in Equation 4 aims to find the visual token subset  $V_k$  that maximizes the expected reward of the final answer  $y$ , marginalized over all possible future reasoning paths. However, directly optimizing Equation 4 is intractable at test time, as it requires (i) access to the true reward function  $R$ , which is only available after generating the final answer, and (ii) enumerating over the exponentially large space of visual token subsets and future trajectories.

**Tractable test-time optimization.** To circumvent the chal-

lenge of directly optimizing Equation 4, we reformulate the problem by introducing a simplifying assumption that leads to a tractable test-time objective. Specifically, we adopt a Markov assumption, positing that the utility of  $V_k$  at step  $k$  depends primarily on the current reasoning state  $z_k$  rather than the entire reasoning history  $\tau_{1:k-1}$ . This is reasonable since  $z_k$  is generated autoregressively conditioned on  $\tau_{1:k-1}$ , thus implicitly encoding the relevant historical context. With this assumption, we replace the intractable expected reward in Equation 4 with a tractable proxy test-time objective:

$$\tilde{V}_k = \arg \max_{V_k \subseteq \mathcal{V}} \mathcal{J}(V_k | x_{\text{input}}, z_k), \quad (5)$$

where  $\mathcal{J}(V_k | x_{\text{input}}, z_k)$  is a scoring function that helps select the best visual tokens in  $V_k$ .

**Designing the scoring function  $\mathcal{J}$ .** Intuitively, we seek a coreset  $V_k$  whose tokens are not only relevant to the current reasoning step  $z_k$  but also maximally diverse to ensure maximum coverage of the visual content and avoid redundancy. Geometrically, this corresponds to finding tokens whose feature representations, when projected into the subspace defined by  $z_k$ , span the largest volume – ensuring relevance through projection and diversity through volume maximization [11, 28, 40].

To formalize this intuition, we employ Determinantal Point Processes (DPPs) [28, 40], a probabilistic framework that naturally captures both relevance and diver-

sity through a kernel-based determinant. Let  $z_k = \{z_k^{(1)}, z_k^{(2)}, \dots, z_k^{(T_k)}\} \in \mathbb{R}^{T_k \times d}$  denote the  $T_k$  text token embeddings in reasoning state  $z_k$ . We capture the reasoning subspace geometry via:

$$M_k = \sum_{i=1}^{T_k} z_k^{(i)} (z_k^{(i)})^\top. \quad (6)$$

We then define a positive semi-definite similarity kernel that measures how similar any pair of visual tokens  $v_i, v_j$  appear when projected into this textual subspace  $L_k(v_i, v_j) = \phi_k(v_i)^\top \phi_k(v_j)$  where  $\phi_k(v) = M_k^{1/2} v$  embeds the visual token  $v$  into a feature space aligned with the geometry of the reasoning subspace spanned by  $z_k$ . Using this kernel, we define our scoring function as the determinant of the kernel matrix restricted to subset  $V_k$ :

$$\mathcal{J}(V_k | x_{\text{input}}, z_k) = \det(L_k^{V_k}), \quad (7)$$

where  $L_k^{V_k} \in \mathbb{R}^{|V_k| \times |V_k|}$  is the kernel matrix restricted to the subset  $V_k$ , with entries  $[L_k^{V_k}]_{ij} = L_k(v_i, v_j)$  for  $v_i, v_j \in V_k$ . The determinant naturally balances relevance and diversity: it increases when tokens are individually relevant to  $z_k$  (high diagonal values) while penalizing redundancy through the correlation structure (off-diagonal terms). By jointly considering Equations 5 and 7, our final optimization becomes:

$$\tilde{V}_k = \arg \max_{V_k \subseteq \mathcal{V}} \det(L_k^{V_k}). \quad (8)$$

**Why maximizing the determinant works?** Maximizing  $\log \det(L_k^{V_k})$  in Equation (8) explicitly balances relevance and diversity. For each visual token  $v_i$ , we define its relevance to the current reasoning state  $z_k$  as

$$r_i^2 = \phi_k(v_i)^\top \phi_k(v_i) = v_i^\top M_k v_i = \sum_{j=1}^{T_k} (v_i^\top z_k^{(j)})^2, \quad (9)$$

which measures the alignment between token  $v_i$  and the text-conditioned representation  $z_k$ . We also define a normalized diversity kernel  $[\bar{L}_k]_{ij} = [L_k]_{ij} / (r_i r_j)$ , so that  $\forall V_k$ , the kernel matrix factorizes as  $L_k^{V_k} = \text{Diag}(r_{V_k}) \bar{L}_k^{V_k} \text{Diag}(r_{V_k})$ , yielding (full derivation in Appendix):

$$\log \det(L_k^{V_k}) = \underbrace{\sum_{v_i \in V_k} \log(r_i^2)}_{\text{relevance}} + \underbrace{\log \det(\bar{L}_k^{V_k})}_{\text{diversity}}. \quad (10)$$

This decomposition reveals that our objective naturally balances: (1) the *relevance term*, measuring the overall alignment of selected visual tokens with the textual context, and (2) the *diversity term*, ensuring selected tokens are mutually dissimilar ensuring maximum visual coverage.

---

### Algorithm 1 VISREF: Visual Refocusing while Thinking

---

**Require:** Image-text input  $x_{\text{input}} = [I, T]$ , visual tokens  $\mathcal{V} = \{v_1, \dots, v_N\}$ , token budget  $m$ , entropy threshold  $\delta_{\text{entropy}}$ , maximum steps  $K_{\text{max}}$

**Ensure:** Final answer  $y$

- 1: Initialize  $k \leftarrow 1, \tau \leftarrow \emptyset$
  - 2: **while**  $k \leq K_{\text{max}}$  **do**
  - 3:     // Generate reasoning step
  - 4:     Sample  $z_k \sim \pi_\theta(\cdot | x_{\text{input}}, \tau_{1:k-1})$
  - 5:     // Select relevant and diverse visual tokens (Section 4.1.1)
  - 6:     Compute text subspace:  $M_k = \sum_{j=1}^{T_k} z_k^{(j)} (z_k^{(j)})^\top$
  - 7:     Define kernel:  $L_k(v_i, v_j) = v_i^\top M_k v_j$
  - 8:      $\tilde{V}_k \leftarrow$  Greedy selection of  $m$  tokens via Eq. (11)
  - 9:     // Update trajectory
  - 10:      $\tau_{1:k} \leftarrow \tau_{1:k-1} \cup \{(z_k, \tilde{V}_k)\}$
  - 11:     // Check stopping criterion (Section 4.1.2)
  - 12:      $H_k \leftarrow -\mathbb{E}_{y \sim \pi_\theta} [\log \pi_\theta(y | x_{\text{input}}, \tau_{1:k})]$
  - 13:     **if**  $H_k < \delta_{\text{entropy}}$  **then**
  - 14:         **break**
  - 15:      $k \leftarrow k + 1$
  - 16:     // Generate final answer
  - 17:     Sample  $y \sim \pi_\theta(\cdot | x_{\text{input}}, \tau_{1:k})$
  - 18: **return**  $y$
- 

**Efficient inference-time solution.** The combinatorial optimization in Equation (8) is NP-hard [27]. Hence, following prior works [7, 55], we approximate the solution via a greedy selection algorithm. We introduce a token budget  $m$  that controls the number of visual tokens selected at each reasoning step, enforcing  $|V_k| = m$ . Starting from  $V_k^{(0)} = \emptyset$ , at iteration  $i$  we select the token with maximum marginal gain:

$$v_{k,i} = \arg \max_{v \in \mathcal{V} \setminus V_k^{(i-1)}} \left[ \log \left( \frac{\det(L_k^{V_k^{(i-1)} \cup \{v\}})}{\det(L_k^{V_k^{(i-1)}})} \right) \right] \quad (11)$$

and update  $V_k^{(i)} \leftarrow V_k^{(i-1)} \cup \{v_{k,i}\}$ . We terminate after  $m$  iterations, setting  $\tilde{V}_k \leftarrow V_k^{(m)}$ .

#### 4.1.2. Adaptive Stopping Criterion

Beyond selecting the optimal visual tokens, the framework must also determine when to terminate reasoning and produce the final answer. For this, we propose an adaptive stopping criterion based on the model’s predictive confidence. At each reasoning step  $k$ , given the current visual-integrated trajectory  $\tau_{1:k} = \{(z_1, V_1), \dots, (z_k, V_k)\}$ , we assess the model’s certainty by measuring the entropy of its response distribution, defined as  $H_k = -\mathbb{E}_{y \sim \pi_\theta(\cdot | x_{\text{input}}, \tau_{1:k})} [\log \pi_\theta(y | x_{\text{input}}, \tau_{1:k})]$ . A low entropy  $H_k < \delta_{\text{entropy}}$ , where  $\delta_{\text{entropy}}$  is a threshold hyperparameter, signals that the model has converged to a confident answer distribution where further reasoning is unlikely to yield improvement. Conversely, high

Table 1. **Evaluation on visual reasoning benchmarks.** We evaluate VISREF across three visual reasoning benchmarks. To ensure a fair comparison, all methods adopt the adaptive stopping criterion described in Section 4.1.2. For brevity, we denote *Standard Thinking* as **ST**, and *Textual Self-Reflection* [34] as **TSR**. All results are reported in accuracy (%), and the numbers in parentheses indicate the performance gain over the ST baseline.

Model	Method	MathVision	MathVista	MM-Star
InternVL3.5-8B	ST (Baseline)	39.2	68.1	57.2
	TSR [34]	40.1	73.9	58.3
	<b>VisRef (Ours)</b>	<b>44.6 (+4.5)</b>	<b>79.3 (+5.4)</b>	<b>63.1 (+4.8)</b>
Qwen3-VL-8B	ST (Baseline)	53.8	74.1	66.5
	TSR [34]	54.3	74.2	65.9
	<b>VisRef (Ours)</b>	<b>56.6 (+2.3)</b>	<b>77.1 (+2.9)</b>	<b>69.1 (+3.2)</b>
SAIL-VL2-8B	ST (Baseline)	29.8	73.1	47.7
	TSR [34]	31.9	73.8	48.9
	<b>VisRef (Ours)</b>	<b>37.3 (+5.4)</b>	<b>78.2 (+4.4)</b>	<b>55.3 (+6.4)</b>

entropy indicates uncertainty and the potential benefit of additional reasoning steps with visual refocusing. To bound computation, we enforce a maximum number of reasoning steps,  $K_{\max}$ . This criterion naturally adapts to problem difficulty: simpler questions reach low entropy quickly, while complex problems utilize extended reasoning before achieving sufficient confidence. After termination of the reasoning trajectory, the final answer is generated as:  $y \sim \pi_{\theta}(\cdot | x_{\text{input}}, \tau_k)$ .

The complete framework, combining our visual token selection (Section 4.1.1) with the adaptive stopping criterion (Section 4.1.2), is summarized in Algorithm 1.

## 5. Experiments

**Experimental Setup.** We evaluate VISREF on three visual reasoning benchmarks—MathVista [33] (*testmini*, 1,000 problems), MathVision [43] (304 competition-style problems), and MM-Star [8] (1,500 vision-dependent questions)—using three state-of-the-art MLRMs in their reasoning (*thinking*) mode: InternVL3.5-8B [45], SAIL-VL2-Thinking [56], and Qwen-3-VL-8B-Thinking [4]. We compare against (i) Standard Thinking (ST; Eq. 1) and (ii) Textual Self-Reflection (TSR) [34]; unless otherwise stated, we set the adaptive stopping entropy threshold  $\delta_{\text{entropy}}=0.25$ , visual token budget  $m = \lfloor 0.3|\mathcal{V}| \rfloor$ , and maximum reasoning steps  $K_{\max}=10$ . We report test accuracy by checking whether each model’s final prediction  $y$  matches the ground-truth answer  $y^*$  for each image-text input. A detailed description is provided in the Appendix.

**Evaluation Results.** Table 1 presents evaluation results across three visual reasoning benchmarks and three MLRMs comparing VISREF with standard thinking (ST), and textual self-reflection (TSR) [34]. To ensure fair comparison, we employ the same adaptive stopping criterion (Section 4.1.2) for textual self-reflection as well. First, we observe that textual self-reflection provides inconsistent im-

provements over standard thinking, with gains ranging from 0.1% to 2.1% on most benchmarks but notably degrading performance by 0.6% on MM-Star with Qwen-3-VL-8B. This inconsistency suggests that purely textual reasoning extension offers limited and unreliable benefits for vision-dependent tasks. In contrast, VISREF consistently outperforms both baselines across all settings. Using InternVL-3.5-8B, VISREF achieves substantial improvements of 5.4%, 11.2%, and 5.9% over standard thinking on MathVision, MathVista, and MM-Star, respectively. Compared to textual self-reflection, VISREF gains an additional 4.5% and 5.4% on MathVision and MathVista respectively. Similar improvements are observed with Qwen-3-VL-8B (2.8%, 3.0%, 2.6%) and SAIL-VL2-8B (7.5%, 5.1%, 7.6%), demonstrating the generalizability of our approach across different model architectures. These results highlight that selective visual token reinjection effectively maintains visual grounding throughout reasoning.

**Understanding test-time scaling behavior.** Recent studies [17, 19] show that given a fixed test-time thinking token budget  $B$ , an efficient utilization approach is to generate multiple parallel chains of thought. Following this, we evaluate how VISREF scales with increased test-time compute by generating  $\mathcal{C}$  parallel visual-integrated thinking traces for a given image-text pair  $x_{\text{input}}$ :  $\tau^{(i)} \sim \pi_{\theta}(\cdot | x_{\text{input}})$ ,  $i = 1, 2, \dots, \mathcal{C}$ , subject to  $\sum_{i=1}^{\mathcal{C}} |\tau^{(i)}| \leq B$ . Each trace  $\tau^{(i)}$  is sampled independently using Algorithm 1. For each reasoning trace  $\tau^{(i)}$ , we generate a final answer  $y^{(i)} \sim \pi_{\theta}(\cdot | \tau^{(i)}, x_{\text{input}})$ , yielding a candidate set  $\mathcal{Y} = \{y^{(1)}, y^{(2)}, \dots, y^{(\mathcal{C})}\}$ . Following self-consistency aggregation [46], we select the final output via majority voting:  $\tilde{y} = \arg \max_{y \in \mathcal{Y}} \sum_{i=1}^{\mathcal{C}} \mathbb{I}[y^{(i)} = y]$ , where  $\mathbb{I}$  represents the indicator function.

Figure 3 presents the test-time scaling behavior of VISREF across three visual reasoning benchmarks—MathVision [43], MathVista [32], and MM-Star [8]—and three MLRMs—InternVL-3.5-8B (first row), Qwen-3-VL-8B (second row), and SAIL-VL2 (third row). The star marker ( $\star$ ) denotes the baseline with no additional test-time compute (standard thinking), while each successive circle to the right represents increasing test-time token budget. We compare VISREF against parallel thinking [19, 46], which samples multiple text-only reasoning trajectories without visual refocusing. Across all benchmarks and models, VISREF consistently achieves superior accuracy for any given computational budget. On MM-Star using InternVL-3.5-8B with a budget of 14K thinking tokens, VISREF achieves around 6% higher accuracy compared to parallel thinking, demonstrating the benefit of maintaining visual grounding throughout the reasoning process.

**Comparison with training-based methods.** Table 2 compares VISREF with Look-Back [51] using InternVL-3.5-8B. While Look-Back achieves strong performance through RL fine-tuning, VISREF attains competitive results *entirely without training*. Moreover, combining Look-Back [1] with VISREF yields the best performance across all benchmarks,

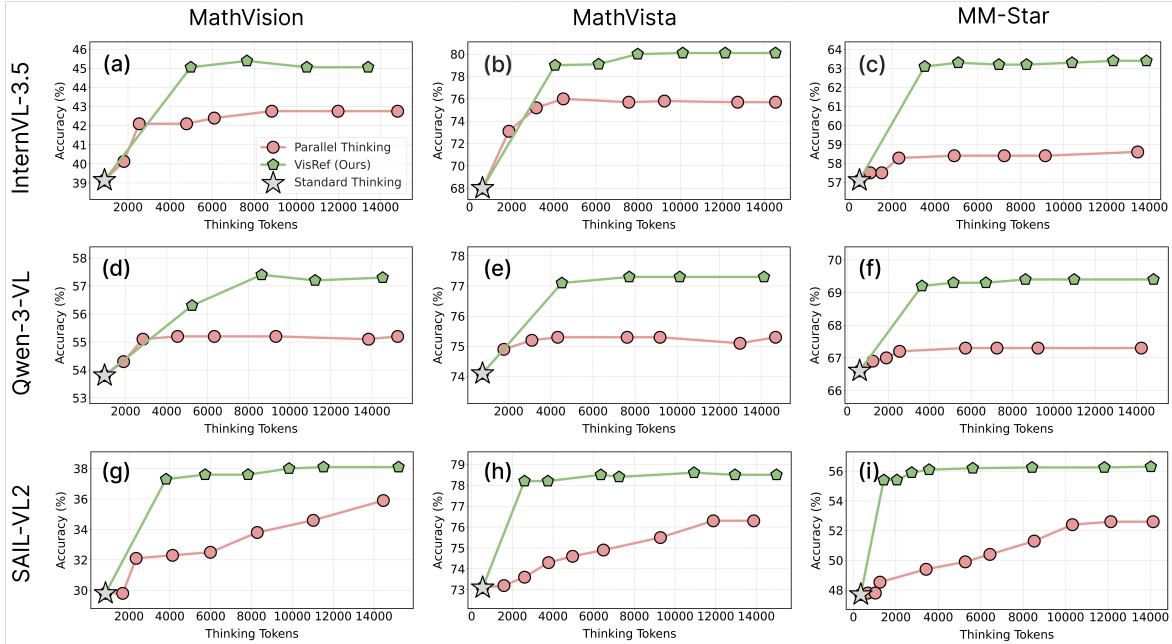


Figure 3. **Test-time scaling of VisREF.** We evaluate the test-time scaling behavior of VisREF by generating multiple parallel visual-integrated reasoning chains under a fixed token budget. Results are shown across three benchmarks (MathVision, MathVista, and MM-Star) and three MLRMs: InternVL-3.5-8B (first row), Qwen-3-VL-8B (second row), and SAIL-VL2 (third row). The star marker ( $\star$ ) denotes standard thinking—the baseline with no additional test-time compute. Parallel thinking [19, 46] generates multiple parallel chains-of-thought without visual refocusing. Across all models and benchmarks, VisREF consistently achieves superior accuracy for any given computational budget.

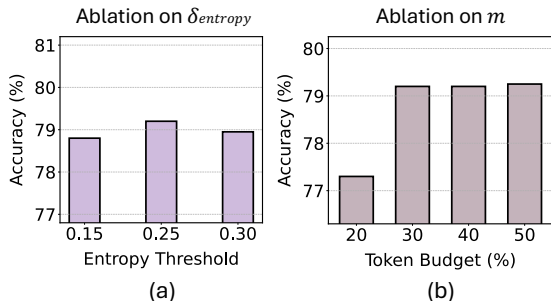


Figure 4. **Ablation study of hyper-parameters.** (a) We visualize the ablation results of the entropy threshold  $\delta_{\text{entropy}}$  used as the stopping criterion. Although the accuracy does not vary significantly across different thresholds, our evaluation shows that  $\delta_{\text{entropy}} = 0.25$  achieves the best balance between accuracy and inference efficiency. (b) We show the ablation of the token budget  $m$  (fraction of visual tokens selected) on MathVista using InternVL-3.5-8B. Accuracy improves from 76.1% to 79.2% as  $m$  increases from 20% to 30% but plateaus for  $m \geq 30\%$ .

demonstrating that our approach is orthogonal to training-based methods and can provide complementary gains. Crucially, VisREF is training-free and can be immediately applied to any pretrained MLRM, whereas Look-Back requires fine-tuning for 60 GPU hours with A6000.

**Comparison with training-based methods.** Table 2 compares VisREF with Look-Back [1] using InternVL-3.5-8B.

Table 2. Comparison with training-based method (*i.e.*, Look-Back [51]) across benchmarks using InternVL-3.5-8B.

Method	MathVista [32]	MathVision [43]	MM-Star [8]
ST	68.1	39.2	57.2
Look-Back [51]	80.8	44.2	63.7
VisREF	79.3	44.6	63.1
Look-Back [51]+VisREF	<b>83.1</b>	<b>48.2</b>	<b>66.0</b>

While Look-Back achieves strong performance through RL fine-tuning, VisREF attains competitive results *entirely without training*. Moreover, combining Look-Back [1] with VisREF yields the best performance across all benchmarks, demonstrating that our approach is orthogonal to training-based methods and can provide complementary gains. Crucially, VisREF is training-free and can be immediately applied to any pretrained MLRM, whereas Look-Back [1] requires fine-tuning for 60 GPU hours with A6000.

## 6. Discussion

### Understanding the importance of relevance and diversity.

As formalized in Equation 10, our objective decomposes into two terms: a relevance term that measures the alignment of visual tokens with the current reasoning step  $z_k$ , and a diversity term that ensures a broad coverage of the visual content. We conduct an ablation study to assess the individual importance of each term. Table 3 presents results on InternVL-3.5-8B across three benchmarks. We observe

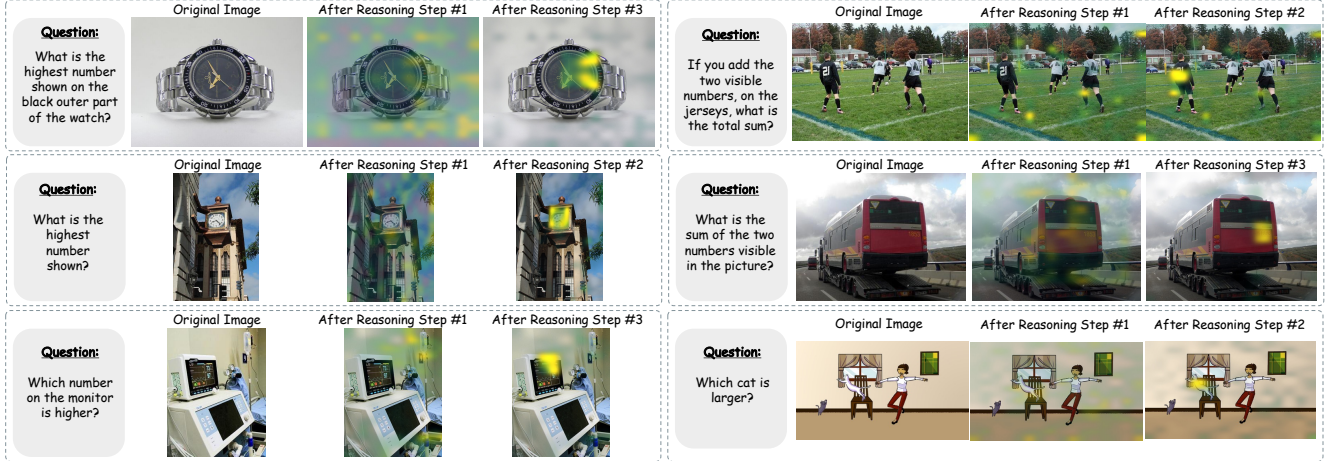


Figure 5. **Attention Visualization.** Attention maps show how VisREF progressively refocuses on relevant visual regions during multi-step reasoning. Initially, the attention maps are noisy. With visual reinjection, VisREF reinforces grounding on task-critical objects, leading to more accurate visual reasoning.

Table 3. **Importance of relevance and diversity.** Ablation study to understand the individual importance of the relevance term and diversity term in our scoring function (Equation 10). We evaluate on InternVL-3.5-8B across all three benchmarks. Accuracy values are reported in percentage (%). Best results are highlighted in **bold**.

Relevance	Diversity	MathVista [32]	MathVison [43]	MM-Star [8]
✓	✗	75.6	43.3	61.0
✗	✓	77.4	42.9	62.8
✓	✓	<b>79.3</b>	<b>44.6</b>	<b>63.1</b>

that the full objective, which jointly optimizes both terms, outperforms variants that use only relevance or only diversity. Notably, using relevance alone results in substantial performance degradation, demonstrating the importance of diversity in selecting effective visual tokens.

**Analysis of entropy threshold.** We analyze the impact of the entropy threshold  $\delta_{\text{entropy}}$ , which determines when to terminate reasoning. Figure 4(a) presents the relationship between accuracy and  $\delta_{\text{entropy}}$  on MathVista using InternVL3.5-8B. While the overall accuracy remains relatively stable across different thresholds, we observe that  $\delta_{\text{entropy}} = 0.25$  consistently yields the highest accuracy across all token budgets. A smaller threshold (e.g., 0.15) requires the model to achieve higher confidence (lower entropy) before stopping, leading to excessive reasoning steps that may introduce overthinking without accuracy gains. Conversely, a larger threshold (e.g., 0.30) can lead to premature termination when the model has insufficient confidence, resulting in under-reasoning and incorrect answer. The same trend is observed for the other two models, Qwen3-VL-8B and SAIL-VL2, demonstrating that this configuration generalizes well across model scales.

**Analysis of token budget.** We next analyze the effect of the token budget  $m$ , which controls the number of visual tokens selected at each reasoning step. Figure 4(b) shows accuracy

as a function of  $m$ . Accuracy increases from 76.1% to 79.2% as  $m$  grows from 20% to 30%, but further increasing  $m$  to 40% yields no additional gains. A similar trend is observed across other models, indicating that VisREF remains robust to different token-budget configurations. Based on these findings, we set  $m = 30\%$  and  $\delta_{\text{entropy}} = 0.25$  for all main experiments, as this configuration achieves a well-balanced trade-off between accuracy and efficiency.

**Qualitative evaluation of VisREF.** To provide deeper insight into how VisREF maintains visual grounding during reasoning, we visualize attention patterns before and after visual refocusing in Figure 5. We present examples from MathVista using InternVL-3.5-8B, where we visualize attention maps across reasoning steps. In the initial reasoning phase without visual refocusing, the attention maps exhibit diffuse and noisy patterns, with the model attending broadly across irrelevant image regions while failing to focus on task-critical visual elements. After applying VisREF’s selective visual token reinjection, the attention patterns become substantially more focused and coherent, concentrating on the objects and regions directly relevant to solving the problem.

## 7. Conclusion

We study how to preserve visual grounding during extended test-time reasoning in multimodal large reasoning models, which tend to overrely on textual priors as the reasoning trace length increases. We propose VisREF, a training-free framework that dynamically reinjects visual information throughout reasoning. Our method selects a compact subset of visual tokens using a DPP-based objective and adaptively terminates reasoning via an entropy-based criterion. Across three visual reasoning benchmarks, under any fixed test-time compute budget, VisREF delivers superior accuracy while remaining efficient by selectively reinjecting visual tokens.

## References

- [1] Manoj Acharya, Kushal Kafle, and Christopher Kanan. Tal-lyqa: Answering complex counting questions. In *Proceedings of the AAAI conference on artificial intelligence*, pages 8076–8084, 2019. 12
- [2] Pranjal Aggarwal and Sean Welleck. L1: Controlling how long a reasoning model thinks with reinforcement learning. *arXiv preprint arXiv:2503.04697*, 2025. 1, 2
- [3] Daman Arora and Andrea Zanette. Training language models to reason efficiently. 2025. 2
- [4] Shuai Bai, Keqin Chen, Xuejing Liu, Jialin Wang, Wenbin Ge, Sibao Song, Kai Dang, Peng Wang, Shijie Wang, Jun Tang, Humen Zhong, Yuanzhi Zhu, Mingkun Yang, Zhaohai Li, Jianqiang Wan, Pengfei Wang, Wei Ding, Zheren Fu, Yiheng Xu, Jiabo Ye, Xi Zhang, Tianbao Xie, Zesen Cheng, Hang Zhang, Zhibo Yang, Haiyang Xu, and Junyang Lin. Qwen2.5-vl technical report. *arXiv preprint arXiv:2502.13923*, 2025. 1, 2, 6, 12
- [5] Lawrence W Barsalou. Grounded cognition. *Annu. Rev. Psychol.*, 59(1):617–645, 2008. 2
- [6] Hardy Chen, Haoqin Tu, Fali Wang, Hui Liu, Xianfeng Tang, Xinya Du, Yuyin Zhou, and Cihang Xie. Sft or rl? an early investigation into training rl-like reasoning large vision-language models, 2025. 2
- [7] Laming Chen, Guoxin Zhang, and Hanning Zhou. Fast greedy map inference for determinantal point process to improve recommendation diversity, 2018. 5
- [8] Lin Chen, Jinsong Li, Xiaoyi Dong, Pan Zhang, Yuhang Zang, Zehui Chen, Haodong Duan, Jiaqi Wang, Yu Qiao, Dahua Lin, et al. Are we on the right way for evaluating large vision-language models? *Advances in Neural Information Processing Systems*, 37:27056–27087, 2024. 1, 2, 6, 7, 8, 12
- [9] Xu Chu, Xinrong Chen, Guanyu Wang, Zhijie Tan, Kui Huang, Wenyu Lv, Tong Mo, and Weiping Li. Qwen look again: Guiding vision-language reasoning models to re-attention visual information. *arXiv preprint arXiv:2505.23558*, 2025. 1, 2, 3, 4
- [10] Jiwan Chung, Junhyeok Kim, Siyeol Kim, Jaeyoung Lee, Min Soo Kim, and Youngjae Yu. Don’t look only once: Towards multimodal interactive reasoning with selective visual revisitation. *arXiv preprint arXiv:2505.18842*, 2025. 3
- [11] Ali Civril and Malik Magdon-Ismail. On selecting a maximum volume sub-matrix of a matrix and related problems. *Theoretical Computer Science*, 410(47-49):4801–4811, 2009. 4
- [12] Andy Clark. Whatever next? predictive brains, situated agents, and the future of cognitive science. *Behavioral and brain sciences*, 36(3):181–204, 2013. 2
- [13] Yihe Deng, Hritik Bansal, Fan Yin, Nanyun Peng, Wei Wang, and Kai-Wei Chang. Openvlthinker: An early exploration to complex vision-language reasoning via iterative self-improvement. *arXiv preprint arXiv:2503.17352*, 2025. 2
- [14] Gongfan Fang, Xinyin Ma, and Xinchao Wang. Thinkless: Llm learns when to think. *arXiv preprint arXiv:2505.13379*, 2025. 2
- [15] Alessandro Favero, Luca Zancato, Matthew Trager, Siddharth Choudhary, Pramuditha Perera, Alessandro Achille, Ashwin Swaminathan, and Stefano Soatto. Multi-modal hallucination control by visual information grounding. In *Proceedings of the IEEE/CVF Conference on Computer Vision and Pattern Recognition*, pages 14303–14312, 2024. 3
- [16] Hao Fei, Shengqiong Wu, Wei Ji, Hanwang Zhang, Meishan Zhang, Mong-Li Lee, and Wynne Hsu. Video-of-thought: Step-by-step video reasoning from perception to cognition. *arXiv preprint arXiv:2501.03230*, 2024. 2
- [17] Yunzhen Feng, Julia Kempe, Cheng Zhang, Parag Jain, and Anthony Hartshorn. What characterizes effective reasoning? revisiting length, review, and structure of cot. *arXiv preprint arXiv:2509.19284*, 2025. 6
- [18] Xinyu Geng, Peng Xia, Zhen Zhang, Xinyu Wang, Qiuchen Wang, Ruixue Ding, Chenxi Wang, Jialong Wu, Yida Zhao, Kuan Li, et al. Webwatcher: Breaking new frontier of vision-language deep research agent. *arXiv preprint arXiv:2508.05748*, 2025. 3
- [19] Soumya Suvra Ghosal, Souradip Chakraborty, Avinash Reddy, Yifu Lu, Mengdi Wang, Dinesh Manocha, Furong Huang, Mohammad Ghavamzadeh, and Amrit Singh Bedi. Does thinking more always help? understanding test-time scaling in reasoning models. *arXiv preprint arXiv:2506.04210*, 2025. 2, 3, 6, 7, 12, 13
- [20] Google DeepMind. Gemini 2.5 Pro: The latest Gemini multimodal model. <https://deepmind.google/technologies/gemini/>, 2024. 2
- [21] Daya Guo, Dejian Yang, Haowei Zhang, Junxiao Song, Ruoyu Zhang, Runxin Xu, Qihao Zhu, Shirong Ma, Peiyi Wang, Xiao Bi, et al. Deepseek-rl: Incentivizing reasoning capability in llms via reinforcement learning. *arXiv preprint arXiv:2501.12948*, 2025. 2, 3
- [22] Michael Hassid, Gabriel Synnaeve, Yossi Adi, and Roy Schwartz. Don’t overthink it. preferring shorter thinking chains for improved llm reasoning. *arXiv preprint arXiv:2505.17813*, 2025. 2
- [23] Shijue Huang, Hongru Wang, Wanjun Zhong, Zhaochen Su, Jiazhan Feng, Bowen Cao, and Yi R Fung. Adactrl: Towards adaptive and controllable reasoning via difficulty-aware budgeting. *arXiv preprint arXiv:2505.18822*, 2025. 2
- [24] Wenxuan Huang, Bohan Jia, Zijie Zhai, Shaosheng Cao, Zheyu Ye, Fei Zhao, Zhe Xu, Yao Hu, and Shaohui Lin. Vision-rl: Incentivizing reasoning capability in multimodal large language models. *arXiv preprint arXiv:2503.06749*, 2025. 2
- [25] Zeyi Huang, Yuyang Ji, Anirudh Sundara Rajan, Zefan Cai, Wen Xiao, Haohan Wang, Junjie Hu, and Yong Jae Lee. Visu-alsoolagent (vista): A reinforcement learning framework for visual tool selection. *arXiv preprint arXiv:2505.20289*, 2025. 3
- [26] Lingjie Jiang, Xun Wu, Shaohan Huang, Qingxiu Dong, Zewen Chi, Li Dong, Xingxing Zhang, Tengchao Lv, Lei Cui, and Furu Wei. Think only when you need with large hybrid-reasoning models. *arXiv preprint arXiv:2505.14631*, 2025. 2
- [27] Chun-Wa Ko, Jon Lee, and Maurice Queyranne. An exact algorithm for maximum entropy sampling. *Operations Research*, 43(4):684–691, 1995. 5

- [28] Alex Kulesza, Ben Taskar, et al. Determinantal point processes for machine learning. *Foundations and Trends® in Machine Learning*, 5(2–3):123–286, 2012. 2, 4
- [29] Yifan Li, Yifan Du, Kun Zhou, Jinpeng Wang, Wayne Xin Zhao, and Ji-Rong Wen. Evaluating object hallucination in large vision-language models. *arXiv preprint arXiv:2305.10355*, 2023. 1
- [30] Zhuowei Li, Haizhou Shi, Yunhe Gao, Di Liu, Zhenting Wang, Yuxiao Chen, Ting Liu, Long Zhao, Hao Wang, and Dimitris N Metaxas. The hidden life of tokens: Reducing hallucination of large vision-language models via visual information steering. *arXiv preprint arXiv:2502.03628*, 2025. 3
- [31] Guosheng Liang, Longguang Zhong, Ziyi Yang, and Xiaojun Quan. Thinkswitcher: When to think hard, when to think fast. *arXiv preprint arXiv:2505.14183*, 2025. 2
- [32] Pan Lu, Hritik Bansal, Tony Xia, Jiacheng Liu, Chunyuan Li, Hannaneh Hajishirzi, Hao Cheng, Kai-Wei Chang, Michel Galley, and Jianfeng Gao. Mathvista: Evaluating mathematical reasoning of foundation models in visual contexts. In *The Twelfth International Conference on Learning Representations*. 1, 2, 3, 4, 6, 7, 8
- [33] Pan Lu, Hritik Bansal, Tony Xia, Jiacheng Liu, Chunyuan Li, Hannaneh Hajishirzi, Hao Cheng, Kai-Wei Chang, Michel Galley, and Jianfeng Gao. Mathvista: Evaluating mathematical reasoning of foundation models in visual contexts. *arXiv preprint arXiv:2310.02255*, 2023. 6, 12
- [34] Niklas Muennighoff, Zitong Yang, Weijia Shi, Xiang Lisa Li, Li Fei-Fei, Hannaneh Hajishirzi, Luke Zettlemoyer, Percy Liang, Emmanuel Candès, and Tatsunori Hashimoto. s1: Simple test-time scaling. *arXiv preprint arXiv:2501.19393*, 2025. 1, 2, 3, 6, 12, 14
- [35] openai. Learning to reason with llms. 2024. 2
- [36] Yingzhe Peng, Gongrui Zhang, Miaosen Zhang, Zhiyuan You, Jie Liu, Qipeng Zhu, Kai Yang, Xingzhong Xu, Xin Geng, and Xu Yang. Lmm-r1: Empowering 3b llms with strong reasoning abilities through two-stage rule-based rl. *arXiv preprint arXiv:2503.07536*, 2025. 2
- [37] Hao Shao, Shengju Qian, Han Xiao, Guanglu Song, Zhuofan Zong, Letian Wang, Yu Liu, and Hongsheng Li. Visual cot: Advancing multi-modal language models with a comprehensive dataset and benchmark for chain-of-thought reasoning. *Advances in Neural Information Processing Systems*, 37:8612–8642, 2024. 2
- [38] Charlie Snell, Jaehoon Lee, Kelvin Xu, and Aviral Kumar. Scaling llm test-time compute optimally can be more effective than scaling model parameters. *arXiv preprint arXiv:2408.03314*, 2024. 2, 3
- [39] Alex Su, Haozhe Wang, Weiming Ren, Fangzhen Lin, and Wenhui Chen. Pixel reasoner: Incentivizing pixel-space reasoning with curiosity-driven reinforcement learning. *arXiv preprint arXiv:2505.15966*, 2025. 3
- [40] Alex Kulesza Ben Taskar. Determinantal point processes for machine learning. *stat*, 1050:10, 2013. 4
- [41] Kimi Team, Angang Du, Bohong Yin, Bowei Xing, Bowen Qu, Bowen Wang, Cheng Chen, Chenlin Zhang, Chenzhuang Du, Chu Wei, et al. Kimi-vl technical report. *arXiv preprint arXiv:2504.07491*, 2025. 2
- [42] Omkar Thawakar, Dinura Dissanayake, Ketan More, Ritesh Thawkar, Ahmed Heakl, Noor Ahsan, Yuhao Li, Mohammed Zumri, Jean Lahoud, Rao Muhammad Anwer, et al. Llamavol: Rethinking step-by-step visual reasoning in llms. *arXiv preprint arXiv:2501.06186*, 2025. 2
- [43] Ke Wang, Junting Pan, Weikang Shi, Zimu Lu, Houxing Ren, Aojun Zhou, Mingjie Zhan, and Hongsheng Li. Measuring multimodal mathematical reasoning with math-vision dataset. In *The Thirty-eight Conference on Neural Information Processing Systems Datasets and Benchmarks Track*, 2024. 2, 6, 7, 8, 12
- [44] Weiyun Wang, Zhangwei Gao, Lixin Gu, Hengjun Pu, Long Cui, Xingguang Wei, Zhaoyang Liu, Linglin Jing, Shenglong Ye, Jie Shao, Zhaokai Wang, Zhe Chen, Hongjie Zhang, Ganlin Yang, Haomin Wang, Qi Wei, Jinhui Yin, Wenhao Li, Erfei Cui, Guanzhou Chen, Zichen Ding, Changyao Tian, Zhenyu Wu, Jingjing Xie, Zehao Li, Bowen Yang, Yuchen Duan, Xuehui Wang, Zhi Hou, Haoran Hao, Tianyi Zhang, Songze Li, Xiangyu Zhao, Haodong Duan, Nianchen Deng, Bin Fu, Yinan He, Yi Wang, Conghui He, Botian Shi, Junjun He, Ying-tong Xiong, Han Lv, Lijun Wu, Wenqi Shao, Kaipeng Zhang, Huipeng Deng, Biqing Qi, Jiaye Ge, Qipeng Guo, Wenwei Zhang, Songyang Zhang, Maosong Cao, Junyao Lin, Kexian Tang, Jianfei Gao, Haian Huang, Yuzhe Gu, Chengqi Lyu, Huanze Tang, Rui Wang, Haijun Lv, Wanli Ouyang, Limin Wang, Min Dou, Xizhou Zhu, Tong Lu, Dahua Lin, Jifeng Dai, Weijie Su, Bowen Zhou, Kai Chen, Yu Qiao, Wenhao Wang, and Gen Luo. Internvl3.5: Advancing open-source multimodal models in versatility, reasoning, and efficiency, 2025. 2, 4
- [45] Weiyun Wang, Zhangwei Gao, Lixin Gu, Hengjun Pu, Long Cui, Xingguang Wei, Zhaoyang Liu, Linglin Jing, Shenglong Ye, Jie Shao, et al. Internvl3. 5: Advancing open-source multimodal models in versatility, reasoning, and efficiency. *arXiv preprint arXiv:2508.18265*, 2025. 6, 12
- [46] Yizhong Wang, Yeganeh Kordi, Swaroop Mishra, Alisa Liu, Noah A Smith, Daniel Khashabi, and Hannaneh Hajishirzi. Self-instruct: Aligning language models with self-generated instructions. *arXiv preprint arXiv:2212.10560*, 2022. 2, 6, 7, 12, 13
- [47] Jason Wei, Xuezhi Wang, Dale Schuurmans, Maarten Bosma, Fei Xia, Ed Chi, Quoc V Le, Denny Zhou, et al. Chain-of-thought prompting elicits reasoning in large language models. *Advances in neural information processing systems*, 35:24824–24837, 2022. 1, 2
- [48] Yuyang Wu, Yifei Wang, Ziyu Ye, Tianqi Du, Stefanie Jegelka, and Yisen Wang. When more is less: Understanding chain-of-thought length in llms. *arXiv preprint arXiv:2502.07266*, 2025. 2
- [49] xAI. Realworldqa, 2024. 12
- [50] Guowei Xu, Peng Jin, Ziang Wu, Hao Li, Yibing Song, Lichao Sun, and Li Yuan. Llava-cot: Let vision language models reason step-by-step. *arXiv preprint arXiv:2411.10440*, 2024. 2
- [51] Shuo Yang, Yuwei Niu, Yuyang Liu, Yang Ye, Bin Lin, and Li Yuan. Look-back: Implicit visual re-focusing in mllm reasoning. *arXiv preprint arXiv:2507.03019*, 2025. 1, 2, 3, 4, 6, 7

- [52] Wenkai Yang, Shuming Ma, Yankai Lin, and Furu Wei. Towards thinking-optimal scaling of test-time compute for llm reasoning. 2025. 2
- [53] Yi Yang, Xiaoxuan He, Hongkun Pan, Xiyan Jiang, Yan Deng, Xingtao Yang, Haoyu Lu, Dacheng Yin, Fengyun Rao, Minfeng Zhu, et al. R1-onevision: Advancing generalized multi-modal reasoning through cross-modal formalization. *arXiv preprint arXiv:2503.10615*, 2025. 1, 2
- [54] Huanjin Yao, Jiaxing Huang, Wenhao Wu, Jingyi Zhang, Yibo Wang, Shunyu Liu, Yingjie Wang, Yuxin Song, Haocheng Feng, Li Shen, et al. Mulberry: Empowering mllm with o1-like reasoning and reflection via collective monte carlo tree search. *arXiv preprint arXiv:2412.18319*, 2024. 2
- [55] Jiacheng Ye, Zhiyong Wu, Jiangtao Feng, Tao Yu, and Lingpeng Kong. Compositional exemplars for in-context learning. In *International Conference on Machine Learning*, pages 39818–39833. PMLR, 2023. 5
- [56] Weijie Yin, Yongjie Ye, Fangxun Shu, Yue Liao, Zijian Kang, Hongyuan Dong, Haiyang Yu, Ding kang Yang, Jiacong Wang, Han Wang, et al. Sail-vl2 technical report. *arXiv preprint arXiv:2509.14033*, 2025. 2, 6, 12
- [57] Xiang Yue, Yuansheng Ni, Kai Zhang, Tianyu Zheng, Ruoqi Liu, Ge Zhang, Samuel Stevens, Dongfu Jiang, Weiming Ren, Yuxuan Sun, et al. Mmmu: A massive multi-discipline multi-modal understanding and reasoning benchmark for expert agi. In *Proceedings of the IEEE/CVF Conference on Computer Vision and Pattern Recognition*, pages 9556–9567, 2024. 1, 2, 3
- [58] Jiarui Zhang, Mahyar Khayatkhoei, Prateek Chhikara, and Filip Ilievski. Mllms know where to look: Training-free perception of small visual details with multimodal llms. *arXiv preprint arXiv:2502.17422*, 2025. 3
- [59] Jiajie Zhang, Nianyi Lin, Lei Hou, Ling Feng, and Juanzi Li. Adaptthink: Reasoning models can learn when to think. *arXiv preprint arXiv:2505.13417*, 2025. 2
- [60] Xintong Zhang, Zhi Gao, Bofei Zhang, Pengxiang Li, Xiaowen Zhang, Yang Liu, Tao Yuan, Yuwei Wu, Yunde Jia, Song-Chun Zhu, et al. Chain-of-focus: Adaptive visual search and zooming for multimodal reasoning via rl. *arXiv preprint arXiv:2505.15436*, 2025. 3
- [61] Xiaoyun Zhang, Jingqing Ruan, Xing Ma, Yawen Zhu, Haodong Zhao, Hao Li, Jiansong Chen, Ke Zeng, and Xunliang Cai. When to continue thinking: Adaptive thinking mode switching for efficient reasoning. *arXiv preprint arXiv:2505.15400*, 2025. 2
- [62] Yi-Fan Zhang, Huanyu Zhang, Haochen Tian, Chaoyou Fu, Shuangqing Zhang, Junfei Wu, Feng Li, Kun Wang, Qingsong Wen, Zhang Zhang, et al. Mme-realworld: Could your multi-modal llm challenge high-resolution real-world scenarios that are difficult for humans? *arXiv preprint arXiv:2408.13257*, 2024. 2
- [63] Zhuosheng Zhang, Aston Zhang, Mu Li, Hai Zhao, George Karypis, and Alex Smola. Multimodal chain-of-thought reasoning in language models. *arXiv preprint arXiv:2302.00923*, 2023. 2
- [64] Yu Zhao, Huifeng Yin, Bo Zeng, Hao Wang, Tianqi Shi, Chenyang Lyu, Longyue Wang, Weihua Luo, and Kaifu Zhang. Marco-o1: Towards open reasoning models for open-ended solutions. *arXiv preprint arXiv:2411.14405*, 2024. 2
- [65] Yiyang Zhou, Chenhang Cui, Jaehong Yoon, Linjun Zhang, Zhun Deng, Chelsea Finn, Mohit Bansal, and Huaxiu Yao. Analyzing and mitigating object hallucination in large vision-language models. *arXiv preprint arXiv:2310.00754*, 2023. 1, 3

## Appendix

### A. Limitations

Although VISREF provides consistent improvements across a variety of visual-reasoning benchmarks and model architectures, it introduces additional computational overhead. In particular, applying DPP-based token selection at every reasoning step increases inference latency compared to standard decoding. This accuracy–latency trade-off is inherent to test-time scaling methods; however, our approach offers higher accuracy for a given computational budget than existing alternatives.

### B. Software and Hardware

We run all experiments with Python 3.10.18, PyTorch 2.7.0, and Transformers 4.55.0. For all experimentation, we use four Nvidia A10G GPUs.

### C. Baselines and Implementation Details.

For evaluation, we compare VISREF with two baselines: (1) standard thinking (Equation 1), where the model generates a single reasoning trace without additional intervention, and (2) textual self-reflection [34], which extends reasoning through text-only reflection without visual refocusing. Based on ablations (Section 5), we set the adaptive stopping entropy threshold  $\delta_{\text{entropy}} = 0.25$ , the visual token budget  $m = \lfloor 0.3|\mathcal{V}| \rfloor$  (i.e., 30% of the total visual tokens  $\mathcal{V}$ ), and the maximum reasoning steps  $K_{\text{max}} = 10$ .

### D. Evaluation Criteria.

To evaluate reasoning performance, we report the accuracy of each model on the test set of each dataset. Specifically, for each image-text input  $x_{\text{input}} = [I, T] \in \mathcal{D}^{\text{test}}$ , the model first generates a thinking trace  $\tau$ , followed by the final answer  $y$ . The accuracy metric is defined as:  $\mathbb{E}_{x_{\text{input}} \sim \mathcal{D}^{\text{test}}, \tau \sim \pi_{\theta}(\cdot | x_{\text{input}}), y \sim \pi_{\theta}(\cdot | x_{\text{input}}, \tau)} [\mathbb{1}\{y = y^*\}]$ , where  $y^*$  is the correct answer.

**Datasets & Models.** To validate the effectiveness of VISREF, we conduct experiments on three visual reasoning benchmarks. **MathVista** [33] unifies 31 visual-math datasets covering puzzles, functional plots, and scientific figures to assess diverse mathematical reasoning skills in visual contexts; we use the *testmini* split containing 1,000 problems. **Math-Vision** [43] includes 304 visually grounded math competition problems across 16 disciplines and five difficulty levels, enabling fine-grained evaluation of visual mathematical reasoning. **MM-Star** [8] is a human-curated benchmark of 1,500 vision-dependent questions designed to assess six core multimodal capabilities across 18 detailed axes, including perception, spatial reasoning, and commonsense understanding. We evaluate VISREF on three state-of-the-art

MLRMs—InternVL3.5-8B [45], SAIL-VL2-Thinking [56], and Qwen-3-VL-8B-Thinking [4]—all evaluated in their reasoning (“thinking”) mode, which generates explicit reasoning traces before producing the final answer.

### E. Additional Results

In the main paper (Section 5), we evaluated VISREF on three visual reasoning benchmarks. Here, we extend our evaluation to two additional benchmarks: TallyQA [1] and RealWorldQA [49]. TallyQA [1] focuses on complex counting tasks in visual scenes, requiring models to identify and enumerate multiple objects while maintaining spatial awareness. This benchmark is particularly challenging as it tests whether models can preserve precise visual grounding throughout iterative counting processes. RealWorldQA [49] is designed to evaluate real-world visual understanding using over 700 images, including anonymized vehicular footage and diverse real-world scenes. This benchmark tests models’ abilities to reason about authentic, uncurated visual scenarios encountered in everyday settings. Table 4 presents results on these benchmarks. On TallyQA, VISREF achieves substantial improvements across all three models, with gains of 5.1%, 4.6%, and 5.4% for InternVL3.5-8B, Qwen3-VL-8B, and SAIL-VL2-8B respectively, compared to standard thinking. Similarly, RealWorldQA shows consistent improvements ranging from 2.6% to 3.9% across the model suite, demonstrating VISREF’s effectiveness on real-world visual understanding tasks. Figure 6 illustrates the test-time scaling behavior of VISREF across both additional benchmarks using three MLRMs: InternVL-3.5-8B (top row), Qwen3-VL-8B (middle row), and SAIL-VL2-8B (bottom row). The star marker ( $\star$ ) indicates the baseline with no additional test-time compute (standard thinking), while successive circles represent increasing test-time token budgets. We compare VISREF against parallel thinking [19, 46], which samples multiple text-only reasoning trajectories without visual refocusing. Across all benchmarks and models, VISREF consistently achieves superior accuracy for any given computational budget.

### F. Additional Qualitative Evaluations

To provide deeper insights into how VISREF maintains visual grounding during reasoning, we visualize attention patterns before and after visual refocusing in Figure 7. The visualizations use images from the RealWorldQA [49] dataset with the InternVL-3.5-8B model. We observe that after applying VISREF’s visual token reinjection, the attention patterns become substantially more focused on task-relevant regions, confirming that our method effectively counteracts visual token dilution during extended reasoning chains.

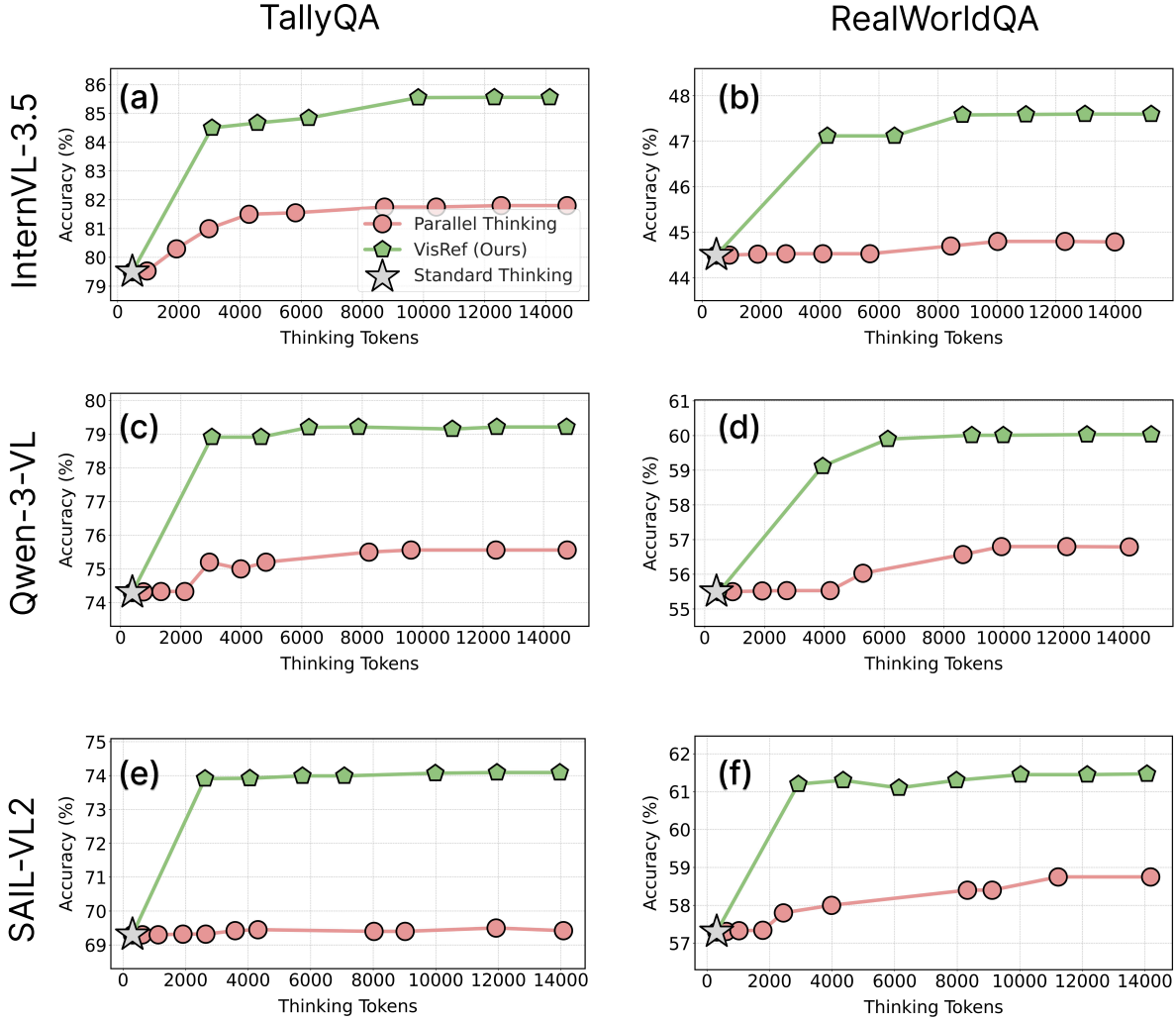


Figure 6. **Test-time scaling of VisREF.** We evaluate the test-time scaling behavior of VisREF by generating multiple parallel visual-integrated reasoning chains under a fixed token budget. Results are shown across two benchmarks (TallyQA, and RealWorldQA) and three MLRMs: InternVL-3.5-8B (first row), Qwen-3-VL-8B (second row), and SAIL-VL2 (third row). The star marker ( $\star$ ) denotes standard thinking—the baseline with no additional test-time compute. Parallel thinking [19, 46] generates multiple parallel chains-of-thought without visual refocusing. Across all models and benchmarks, VisREF consistently achieves superior accuracy for any given computational budget.

## G. Derivation of the Relevance-Diversity Decomposition

In this section, we provide the complete derivation of Equation 10 from the main paper, which decomposes the log-determinant of the kernel matrix into relevance and diversity terms. Specifically, given the kernel matrix  $L_k^{V_k} \in \mathbb{R}^{|V_k| \times |V_k|}$  restricted to visual token subset  $V_k$ , the log-determinant can be decomposed as:

$$\log \det(L_k^{V_k}) = \sum_{v_i \in V_k} \log(r_i^2) + \log \det(\bar{L}_k^{V_k}) \quad (12)$$

where  $r_i$  denotes the relevance score of token  $v_i$ , and  $\bar{L}_k^{V_k}$  is the normalized diversity kernel.

**Derivation.** For any selected subset  $V_k = \{v_1, \dots, v_m\} \subseteq \mathcal{V}$ , the kernel matrix entries are given by:

$$[L_k^{V_k}]_{ij} = L_k(v_i, v_j) = \phi_k(v_i)^\top \phi_k(v_j) = v_i^\top M_k v_j \quad (13)$$

where  $\phi_k(v) = M_k^{1/2} v$  projects visual token  $v$  into the textual reasoning subspace defined by  $M_k = \sum_{j=1}^{T_k} z_k^{(j)} (z_k^{(j)})^\top$ .

The relevance of token  $v_i$  to the current reasoning state  $z_k$  is measured by:

$$r_i^2 = \|\phi_k(v_i)\|_2^2 = v_i^\top M_k v_i = \sum_{j=1}^{T_k} (v_i^\top z_k^{(j)})^2 \quad (14)$$

This quantity captures the alignment between visual token  $v_i$  and the textual context, with  $r_i^2 = [L_k^{V_k}]_{ii}$ . Next, we

Table 4. **Evaluation on additional visual reasoning benchmarks.**

We evaluate VISREF across three visual reasoning benchmarks: TallyQA, and RealQA. To ensure a fair comparison, all methods adopt the adaptive stopping criterion described in Section 4.1.2. For brevity, we denote *Standard Thinking* as **ST**, and *Textual Self-Reflection* [34] as **TSR**. All results are reported in accuracy (%), and the numbers in parentheses indicate the performance gain over the ST baseline.

Model	Method	TallyQA	RealWorldQA
InternVL3.5-8B	ST (Baseline)	79.4	44.6
	TSR [34]	79.6	44.9
	<b>VisRef (Ours)</b>	<b>84.5 (+5.1)</b>	<b>47.2 (+2.6)</b>
Qwen3-VL-8B	ST (Baseline)	74.3	55.4
	TSR [34]	75.1	56.9
	<b>VisRef (Ours)</b>	<b>78.9 (+4.6)</b>	<b>59.1 (+3.7)</b>
SAIL-VL2-8B	ST (Baseline)	69.3	57.3
	TSR [34]	71.7	58.0
	<b>VisRef (Ours)</b>	<b>73.9 (+5.4)</b>	<b>61.2 (+3.9)</b>

introduce the normalized kernel  $\bar{L}_k^{V_k}$  with entries:

$$[\bar{L}_k^{V_k}]_{ij} = \frac{[L_k^{V_k}]_{ij}}{r_i r_j} = \frac{\phi_k(v_i)^\top \phi_k(v_j)}{\|\phi_k(v_i)\|_2 \|\phi_k(v_j)\|_2} \quad (15)$$

Note that  $[\bar{L}_k^{V_k}]_{ii} = 1$  for all  $i$ , representing normalized correlations between tokens. Let  $D_{V_k} = \text{diag}(r_1, \dots, r_m)$ . The kernel matrix can then be factorized as:

$$L_k^{V_k} = D_{V_k} \bar{L}_k^{V_k} D_{V_k} \quad (16)$$

Thus, we can write each element as:  $[D_{V_k} \bar{L}_k^{V_k} D_{V_k}]_{ij} = r_i \cdot \frac{[L_k^{V_k}]_{ij}}{r_i r_j} \cdot r_j = [L_k^{V_k}]_{ij}$ . Applying the multiplicative property of determinants:

$$\det(L_k^{V_k}) = \det(D_{V_k})^2 \det(\bar{L}_k^{V_k}) = \left( \prod_{v_i \in V_k} r_i^2 \right) \det(\bar{L}_k^{V_k}) \quad (17)$$

Finally, taking the natural logarithm yields:

$$\log \det(L_k^{V_k}) = \underbrace{\sum_{v_i \in V_k} \log(r_i^2)}_{\text{relevance term}} + \underbrace{\log \det(\bar{L}_k^{V_k})}_{\text{diversity term}} \quad (18)$$

The first term aggregates individual token relevances to the reasoning context, while the second term, through the normalized kernel determinant, penalizes redundancy and encourages diverse visual coverage. This decomposition provides theoretical justification for why maximizing  $\log \det(L_k^{V_k})$  naturally balances both objectives.

## H. Computational cost analysis.

Table 5 reports detailed latency measurements (on 1 H100 GPU) on the Mathvista dataset using InternVL-3.5-8B. On

Method	Time
ST	7.1s
TSR	7.7s
Look-Back [1]	7.6s
VISREF	8.2s

Table 5. Latency per prompt on MathVista.

Model	ST	TSR	VISREF
InternVL-1B	46.1	48.5	<b>52.0</b>
InternVL-2B	52.9	53.7	<b>58.1</b>
InternVL-8B	68.1	73.9	<b>79.3</b>

Table 6. Accuracy (%) across model scales on MathVista.

average, our DPP-based token selection adds only 0.5 secs of overhead compared to Textual self-reflection (TSR), and 1.1 secs compared to standard thinking (ST). Note that ST does not include self-reflection, so it is faster than others. The efficiency of VISREF stems from greedy approximation of Eq. 11.

## I. Generalization Across Model Scales

We study whether VISREF consistently improves multi-step visual reasoning as the backbone model scales. Specifically, we evaluate InternVL models spanning 1B, 2B, and 8B parameters under the same decoding setup and token budget. Table 6 shows that VISREF yields gains over both Standard Thinking (ST) and Textual Self-Reflection (TSR) at every scale: for the 1B model, VISREF improves accuracy from 46.1% (ST) and 48.5% (TSR) to 52.0%; for 2B, it increases accuracy from 52.9%/53.7% to 58.1%; and for 8B, it improves performance from 68.1%/73.9% to 79.3%. These results suggest that the benefit of visual refocusing is not confined to a particular parameter regime, but instead persists from small to larger models, indicating that VISREF effectively counteracts visual token dilution during extended reasoning across model capacities.

## J. Random Sampling Baseline

We further verify that the improvement of VISREF is not merely due to selecting *any* subset of visual tokens under a fixed budget. To this end, Table 7 compares three selection strategies on InternVL-8B: (i) *Random* selection, (ii) *Relevance-only* selection that greedily keeps the most text-aligned tokens, and (iii) our DPP-based selection that jointly optimizes relevance and diversity. Random selection performs close to the ST baseline and is substantially worse than VISREF across all benchmarks, indicating that naive token subsampling fails to preserve the visual evidence needed for multi-step reasoning. Relevance-only selection improves over random sampling, but it remains consistently below DPP (Ours), suggesting that selecting only the most aligned tokens

Selection	MVista	MVision	MM-Star
Random	67.3	40.8	57.3
Relevance-only	75.6	43.3	61.0
DPP (Ours)	<b>79.3</b>	<b>44.6</b>	<b>63.1</b>

Table 7. Token selection strategies (InternVL-8B).

$\lambda$	0.0 (Div)	0.25	0.5 (Ours)	0.75	1.0 (Rel)
MVista	71.2	76.8	<b>79.3</b>	77.4	75.6
MVision	41.5	43.1	<b>44.6</b>	44.2	43.3

Table 8. Effect of  $\lambda$  weighting (InternVL-8B).

can still be redundant (e.g., repeatedly focusing on similar regions) and may miss complementary evidence elsewhere in the image. By explicitly encouraging diversity in addition to relevance, DPP (Ours) achieves the best results, supporting our claim that balancing relevance and diversity is essential for effective visual refocusing under tight token budgets.

### K. Weighted Version of Eq. 10

We additionally experimented with a weighted objective of the form  $\lambda \cdot \text{relevance} + (1-\lambda) \cdot \text{diversity}$ . As shown in Table 8, performance peaks at  $\lambda=0.5$  across both MathVista and MathVision, indicating that balancing relevance and diversity is important in practice. This result supports our default (unweighted) formulation in the main paper, where the two terms contribute equally.



Figure 7. **Attention Visualization.** Attention maps show how VisREF progressively refocuses on relevant visual regions during multi-step reasoning. Initially, the attention maps are noisy. With visual reinjection, VisREF reinforces grounding on task-critical objects, leading to more accurate visual reasoning.